Static and dynamic depinning processes of a magnetic domain wall from a pinning potential

Ung-Hwan Pi,* Young-Jin Cho, Ji-Young Bae, Sung-Chul Lee, and Sunae Seo
Samsung Electronics Co., San 14-1 Nongseo-dong, Giheung-gu, Yongin-si, Gyeonggi-do 446-712, Republic of Korea

Woojin Kim, Jung-Hwan Moon, and Kyung-Jin Lee
Department of Materials Science and Engineering, Korea University, Seoul 136-713, Republic of Korea

Hyun-Woo Lee
Department of Physics, Pohang University of Science and Technology, Kyungbuk 790-784, Republic of Korea
(Received 2 June 2011; published 15 July 2011)

We investigate experimentally pinning and depinning dynamics of a magnetic domain wall (DW) from a notch in a magnetic nanowire. When the domain wall is initially located at the notch, the domain wall depinning from the notch occurs at a well-defined threshold field. On the other hand, a completely different depinning dynamics is observed when an initially moving DW is pushed to pass through a notch. The depinning probability oscillates with increasing field, and the averaged depinning probability over the oscillation period decreases with increasing field in certain field ranges. These properties are attributed to the coupled dynamics of the DW propagation and the DW polarity reversal.

DOI: 10.1103/PhysRevB.84.024426 PACS number(s): 75.60.Ch, 75.78.Fg

I. INTRODUCTION

The field- or current-driven motion of a magnetic domain wall (DW) in nanostructures opens important prospects for applications in logic[1] and memory devices.[2] Accurate and reproducible control of DW positions is one of the fundamental challenges for the realization of such spintronic devices. DW positioning may be facilitated by introducing structural notches [2] or geometrical curvature.[3] Such structures in magnetic nanowires introduce pinning potentials for a DW, and a thorough understanding of DW pinning and depinning dynamics near the potential well is a subject of great importance.

Two different types of pinning or depinning processes are relevant for the DW position control. One is the static pinning (depinning) process where a DW is initially trapped in a potential well and stays pinned in the well (gets depinned from the well) upon the application of a magnetic field or current. The other is the dynamic pinning (depinning) process where an initially moving DW approaches a potential well and gets trapped at the well (passes through the well). From the application point of view, the differentiation between the two pinning or depinning processes is important since a movement of a DW comprises a static depinning from a pinning potential and a consecutive dynamic pinning in the next pinning potential.

From a viewpoint of fundamental physics, the dynamic depinning processes are expected to be substantially different from the static depinning by two reasons. First, it is known empirically that the static friction is usually larger than the dynamic (or kinetic) friction. This empirical law seems to hold also for the DW dynamics as evidenced by recent experiments.[4,5] Second, the DW dynamics can exhibit an oscillatory behavior. When a field or current is applied, not only the DW position but also the DW tilting angle shows a temporal evolution. In particular, for a field above a certain threshold called the Walker breakdown (H_{WB}), the DW magnetization keeps precessing.[6,7] Since the effective depth of the notch-shaped pinning potential depends on the magnetization direction of the DW, as reported by Atkinson *et al.*,[8] the oscillatory behavior of DW magnetization can affect the depinning probability as well especially for the dynamic case. There have been several experimental reports about the dynamic DW propagation related to the oscillatory motion of the DW.[5,9] However the pinning sites in these reports are uncontrollable defects induced by the edge roughness of nanowires. For in-depth investigation of the dynamic depinning process, experiments with well-controlled pinning potential are desired. In this article we experimentally demonstrate remarkable features of the static and dynamic depinning processes in a nanowire with an intentionally introduced notch-shaped defect.

II. EXPERIMENTS AND RESULTS

Magnetic nanowires are formed by patterning films of $Ni_{80}Fe_{20}$(20 nm)/Ru(5 nm) deposited on highly resistive Si substrates, with electron beam lithography and Ar ion beam etching. Electrical contact lines to the nanowire are formed from Cr(15 nm)/Au(85 nm), with a photolithography and lift-off process. The cross sectional transmission electron microscopy (TEM) image of the magnetic nanowire with the electrode is shown on the upper right corner of Fig. 1. In the geometry of our nanowire (width = 300 nm, thickness = 20 nm), a vortex DW is stable.[10,11] A triangular-shaped notch of 100 nm depth is formed on one side of the nanowire at the distance l from the left electrode used for DW injection. Measurements are carried out on two magnetic nanowires, which have a notch at different positions, 2 and 4 μm, respectively. The measurement setup of the resistance is shown in Fig. 1. The configuration of the DW inside the nanowire is detected by the change of anisotropic magnetoresistance (AMR) measured by an ac bridge circuit.

We performed the dynamic depinning experiments in a manner similar to Hayashi *et al.*[12] In the beginning, the magnetic state of the nanowire is set to a single domain with the magnetization direction toward $-x$. In the measurement of the dynamic depinning, an external field H_{ext} is applied toward $+x$. Subsequently, a 5-ns-wide negative current pulse is applied

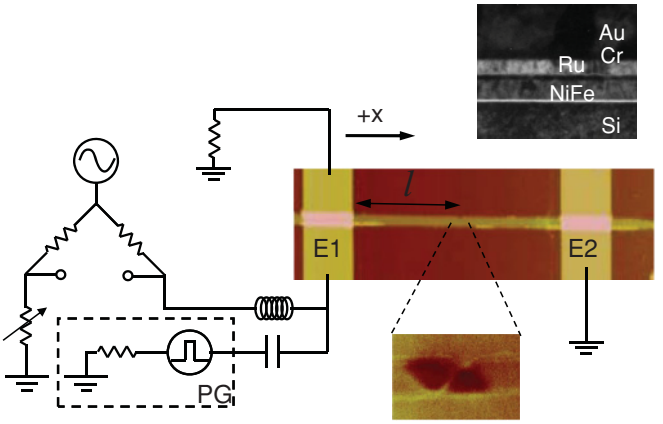

FIG. 1. (Color online) Experimental setup of the resistance measurement of the magnetic nanowire is depicted. A DW is created on the right side of the electrode E1 by a negative current pulse through pulse generator PG. The resistance change of the nanowire is measured through the AC bridge circuit. The cross-sectional TEM image on the upper right corner shows the layer structure of the sample. The blow-up figure of the nanowire is the magnetic force microscopy image obtained after trapping a vortex-type DW.

through the pulse generator for the nucleation of a head-to-head DW. Instantly after the creation, the DW moves toward $+x$ direction by the field H_{ext}. The difference of the AMR values between before and after the nucleation current pulse gives the information about whether the DW has passed or has been trapped and about what kind of structure it is if trapped.

In case of the static depinning process, the current pulse for the nucleation of the DW is applied under a field of 5 Oe. This field is smaller than the Walker breakdown field, which is 6 Oe in our sample, but large enough for the transfer of the DW to the notch because the depinning field of the sample without the notch has been measured to be 2.5 Oe. Thus this procedure prepares a DW trapped at the notch. Subsequent application of H_{ext} then reveals the static depinning process from the notch. The change of AMR values is measured for H_{ext} from 0 to 80 Oe in a step of 0.2 or 0.5 Oe. The measurements at each field value have been repeated 50 times to evaluate the probabilities of depinning, vortex DW trapping, and transverse DW trapping.

Figure 2(a) shows the color-coded histogram of the AMR difference before and after the application of the nucleation current pulse, i.e., $\Delta =$ AMR (after current pulse) $-$ AMR (before current pulse), in a dynamic depinning process on the sample of $l = 4\ \mu$m. Three different levels of Δ are observed, each of which reveals the three different DW states: (1) the DW passes through the notch so that no wall is detected ($\Delta \sim 0\ \Omega$), (2) vortex DW ($\Delta \sim -0.18\ \Omega$), or (3) the transverse DW ($\Delta \sim -0.14\ \Omega$) is pinned at the notch. From the histogram of the Δ shown in Fig. 2(a), the probability of each state can be obtained. The resulting probabilities of the three cases are, respectively, displayed in Fig. 2(b) as black squares, red circles, and blue triangles. The probabilities of the three states are similarly obtained on the static process and displayed in Fig. 2(d). To investigate the effect of the position of the notch, we performed the same measurements on a different sample with different length $l = 2\ \mu$m and depict the results of dynamic process in Fig. 2(e).

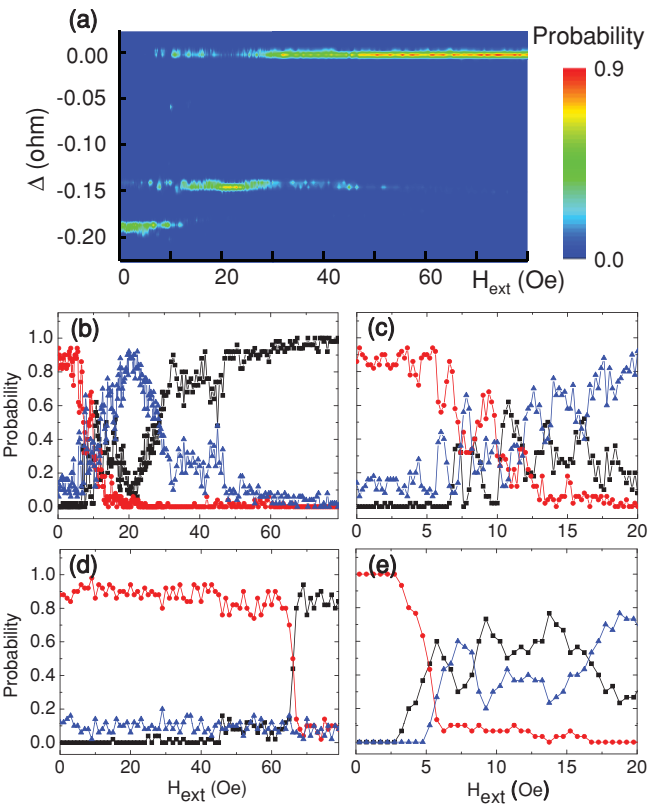

FIG. 2. (Color online) (a) Color-coded histogram of AMR difference between before and after the application of the nucleation current pulse, i.e., $\Delta =$ AMR (after current pulse), $-$ AMR (before current pulse). This has been obtained in a dynamic depinning process on the sample of $l = 4\ \mu$m. (b) Probabilities of the three different cases (1) DW passes through the notch (black square), (2) vortex DW (red circles), or (3) transverse DW (blue triangles) is pinned at the notch are obtained as a function of H_{ext} from the histogram shown in (a). (c) The plot in (b) is magnified in the range 0 Oe $< H_{\text{ext}} <$ 20 Oe to provide clear observation of the oscillatory behavior. (d) The probabilities of the three states presented in (b) are similarly obtained on the static depinning process. It shows a critical difference from (b) obtained in the dynamic depinning process. (e) Dynamic depinning probabilities of the three states are obtained for a sample with $l = 2\ \mu$m. The oscillation period of the probability is much larger than that of (c) obtained with $l = 4\ \mu$m.

The most striking point of the results is the big difference of the depinning behaviors between the dynamic process and the static process. While the depinning probability shows a single jump at $H_{\text{st}} = 65$ Oe in a static process, it begins to increase from about 20 Oe in a dynamic process. This result agrees with the report of Ahn *et al.*[4,5] in that the dynamic depinning field is lower than that of a static depinning field.

A closer look at Fig. 2(b) reveals many interesting features of the dynamic depinning process, which are completely absent for static depinning process. This implies that the difference in the depinning threshold fields between the two processes cannot capture the full difference of the two processes. Below we analyze the properties of the dynamic depinning process, which are the main new findings of this paper. The probability curves in Fig. 2(b) can be clearly classified into two different regions of the applied field

according to their features. Region I is defined as the applied field lower than 20 Oe, where the probability oscillates with the period of about 1 or 2 Oe, and the probability of case 1 (case 3) has a trend to decrease (increase) as H_{ext} goes higher. Region II is the regime of H_{ext} larger than 20 Oe, where vortex DWs are hardly detected and the probability of case 1 (case 3) increases (decreases), contrary to the behavior in the region I. The probability curves of depinning (1) and transverse DW pinning (3) are in an antiphase. It indicates that the transverse DW is more inclined to be pinned than the vortex DW for a given applied field, so that the pinning potential is deeper for the transverse DW than for the vortex DW.

Figure 2(c) shows the region I magnified to provide a clear observation of the oscillatory behavior. From 6.0 Oe, the transverse DW begins to be trapped, indicating that the initial vortex DW begins to transform into a transverse type from this field. We consider this field to be H_{WB} of our sample. Up to about 10 Oe, peaks of case 2 and valleys of case 3 appear at the same applied field because they share the portion of not-depinned events. At above 13 Oe, only the cases 1 and 3 appear with 180° out of phase with each other, and case 2, where the vortex DW is trapped, becomes negligible. In the case of the sample with a different notch position of $l = 2\ \mu$m, the overall behaviors was similar. The probability curve could also be classified into two regions with a boundary at $H_{ext} = 20$ Oe. However, as one can see in Fig. 2(e), the period of oscillation in region I is about 4 Oe, much larger than that of the sample $l = 4\ \mu$m.

III. MICROMAGNETIC CALCULATION AND ANALYSIS

The observed oscillatory probability curves can be explained by continuous transformation of the DW during its propagation accompanied with the Walker breakdown. When the magnetic field is applied along the direction of nanowire length, the core of the vortex DW shifts in the transverse direction during propagation along the direction of applied field. When H_{ext} is larger than H_{WB}, the vortex core disappears to one side of the nanowire, and then it comes back from the same side with opposite polarity.[13–15] The vortex core with the opposite polarity traverses the nanowire to the other side [Fig. 4(d)].

Using micromagnetic modeling,[16] instant trajectories of the vortex cores and the final states of the domain under different H_{ext} have been obtained as shown in Fig. 3. The final state of the DW trapped at the notch depends upon H_{ext}, i.e., the

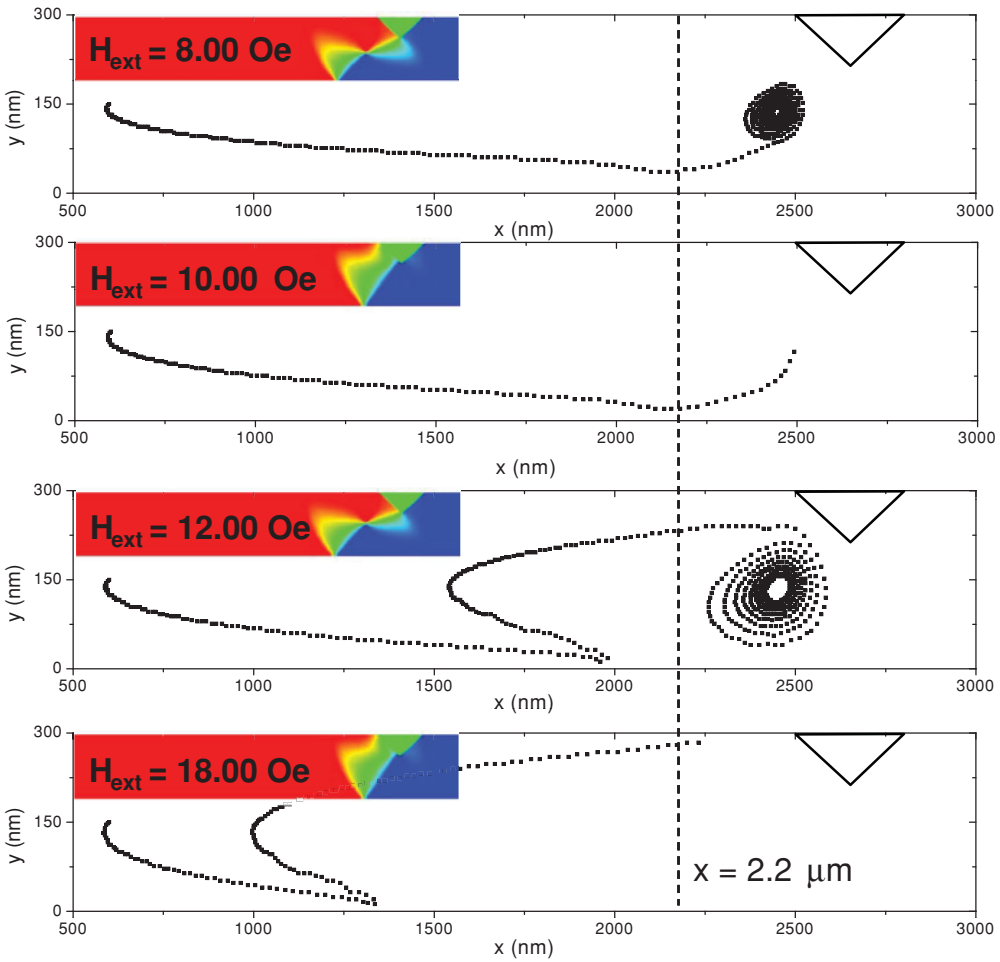

FIG. 3. (Color online) Trajectories of the vortex core from micromagnetic simulation are shown in several fields $H_{ext} = 8$, 10, 12, 18 Oe. The final states of the domain structure are also shown in the inset of each figure of the trajectory to compare the correlation between the trajectory and the structure of the DW trapped at the notch. A dashed line at $x = 2.2\ \mu$m located 400 nm away from the notch center represents a position from which the vortex core begins to be strongly affected by the notch.

vortex DW is trapped at 8 and 12 Oe, while the transverse DW is trapped at 10 and 18 Oe. Comparison of the final state with the trajectory of the vortex core near the notch reveals that the type of DW trapped at the notch is determined by the transverse position (y) of the vortex core when it is around the notch. The crossing points between the trajectory of the vortex core and a dashed line drawn at $x = 2.2$ μm representing a position near the notch show this fact clearly. In case of 10 and 18 Oe, where the transverse DW is trapped, the y value of the crossing point is closer to the side of the nanowire than that of 8 and 12 Oe, where a vortex DW is trapped.

The transverse location of vortex core, when it is near the notch, can be considered as the decisive factor for the state

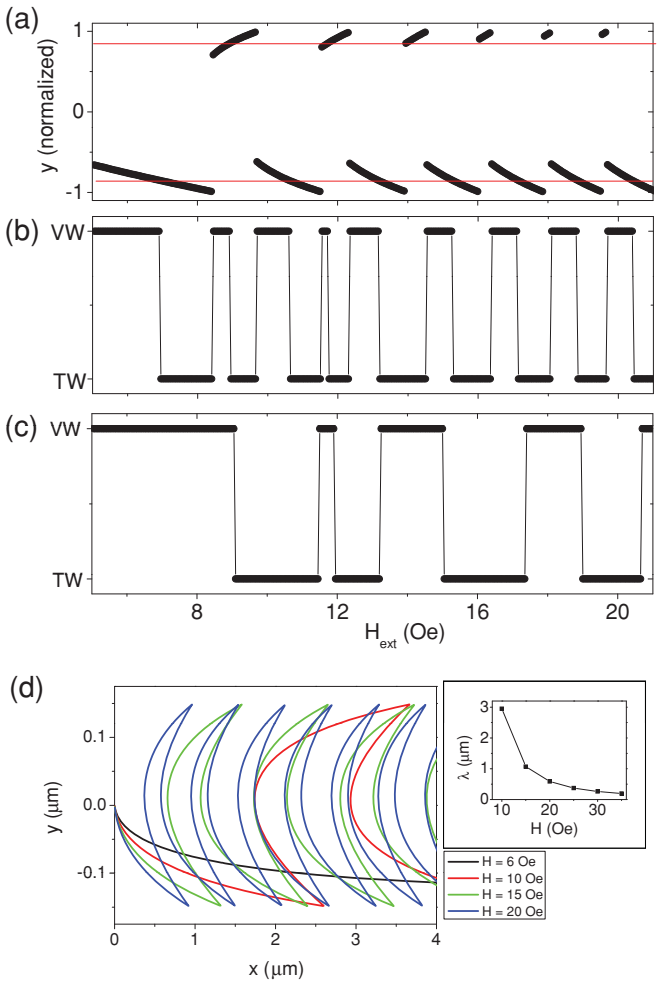

FIG. 4. (Color online) From the analytic equations, the normalized transverse location (y) of a vortex core is calculated when the longitudinal movement (x) of the core along the nanowire is 4 μm. The calculated y position is depicted as a function of H_{ext} in (a). $+1$ and -1 indicate both sides of the nanowire. Two horizontal red lines indicate $+0.85$ and -0.85, respectively. (b) Points in (a) are classified as the vortex wall (VW) ($0.85 < y < +0.85$) and transverse wall (TW) (otherwise). (c) Similar classification of the final DW states has been obtained in the case of a longitudinal movement of 2 μm. (d) The trajectories of the vortex core calculated from analytic equation under several fields H_{ext} are shown. The distance between the two sequential hit on one side of the nanowire is defined as λ, and it is plotted as a function of H_{ext} in the inset.

of the DW at the notch. We estimated the y position of the vortex core when it moves 4 and 2 μm along the nanowire by numerically solving the analytic equations for the location of the vortex core.[14,15,17] The estimated y position obtained after the DW propagation of 4 μm is plotted as a function of H_{ext} in Fig. 4(a). If we assume that a transverse DW is pinned at the notch when the y value is within 15% from each side of the nanowire, an alternating appearance of the two types of DWs is obtained. Such plots obtained for 4 and 2 μm propagations are depicted in Figs. 4(b) and 4(c), respectively. One can notice that the alternating periods are similar to the experimentally observed ones. [See Figs. 2(c) and 2(e).]

Our model calculation explains not only the oscillatory behavior of the pinning and depinning probabilities, but also the variation of the oscillation period by the position of the notch. The notch position-dependent period can be simply understood by the periodic transverse motion of the vortex core. If the frequency of the periodic transverse motion is f, and the time for the DW to reach the notch is τ, the vortex DW transforms into a transverse DW when the phase of the oscillatory core motion is in a certain range, that is, $f\tau = \pi n + \delta$. Here n is integer value corresponding to the number of touches of the core to the edge of the nanowire, and δ is the phase value where the y position exists near the edge of the nanowire. Since f and τ are given by $f = (\gamma/\pi)\sqrt{H_{ext}^2 - H_{WB}^2}$, $\tau = l/v$, respectively,[18] the magnetic field H_{ext} for the structural transformation can be written as $\sqrt{H_{ext}^2 - H_{WB}^2} = (\pi v/\gamma l)(\pi n + \delta)$. Here v, γ are the the velocity of the DW, gyromagnetic ratio, respectively. From this simple equation, one can notice that the oscillation period is nearly inversely proportional to the distance to the notch l, which explains the experimental results very well.

In addition to the oscillatory behavior described above, the probability curves of depinning (1) and its counterpart transverse DW pinning (3) show another interesting behavior. In general, depinning probability is expected to increase as H_{ext} goes higher. This general trend works well in region II ($H_{ext} > 20$ Oe). However, the depinning probability shows an opposite behavior in the field range of $H_{ext} < 20$ Oe. It tends to decrease as the field goes higher in this regime, yielding a minimum depinning probability at $H_{ext} = 20$ Oe.

The trajectory of the vortex core calculated from the analytic equation under several fields is shown in Fig. 4(d). In these plots one can define the distance between the two sequential hits on one side of the nanowire as λ. The plot of λ as a function of H_{ext} is depicted in the inset of Fig. 4(d). It decreases with increasing H_{ext} and becomes smaller than 500 nm at $H_{ext} > 20$ Oe. Here λ can be considered as a wavelength of the wavy motion of the vortex core and is roughly given by the ratio of the velocity to the frequency of the zigzag motion. If we take into account the dependence of the frequency and velocity of the DW on H_{ext} above H_{WB}, one can understand such λ behavior shown in the inset of Fig. 4(d) The smaller λ implies that the vortex core has the more chance to be near the notch when it hits the side of the nanowire. The decreasing probability of the dynamical depinning in the field range $H_{ext} <$ 20 Oe can be understood from the decreasing λ, which is induced by the reduced velocity due to the Walker breakdown.

In region II ($H_{ext} > 20$ Oe), nearly all vortex DWs are transformed into the transverse walls when they are near the

notch, because λ is smaller than 500 nm and comparable to the effective boundary of the influence by the notch. In this field range, the reduction of the pinning potential due to the external field is a decisive factor for the depinning behavior because λ, which has been a crucial role in the field region I, becomes nearly constant value as shown in the inset of Fig. 4(d). Thus the transmission probability increases as H_{ext} goes higher as observed in the experiments.

IV. SUMMARY

To summarize, we have studied the depinning behavior of a DW through the notch. Depending upon the initial condition of the DW, the depinning property showed distinct differences. From the micromagnetic calculation, the complicated feature of the dynamic depinning behavior could be understood by core position-dependent transformation of the DW structure.

*unghwan.pi@samsung.com

[1]D. A. Allwood, G. Xiong, C. C. Faulkner, D. Atkinson, D. Petit, and R. P. Cowburn, Science **309**, 1688 (2005).

[2]S. S. P. Parkin, Masamitsu Hayashi, and Luc Thomas, Science **320**, 190 (2008).

[3]E. Saitoh, H. Miyajima, T. Yamaoka, and G. Tatara, Nature (London) **432**, 203 (2004).

[4]S.-M. Ahn, K.-W. Moon, D.-H. Kim, and S.-B. Choe, Appl. Phys. Lett. **95**, 152506 (2009).

[5]X. Jiang, L. Thomas, R. Moriya, M. Hayashi, B. Bergman, C. Rettner, and S. S. P. Parkin, Nature Communications **1**, 25 (2010).

[6]N. L. Schryer and L. R. Walker, J. Appl. Phys. **45**, 5406 (1974).

[7]G. S. D. Beach, C. Nistor, C. Knutson, M. Tsoi, and J. L. Erskine, Nat. Mater. **4**, 741 (2005).

[8]D. Atkinson, D. S. Eastwood, and L. K. Bogart, Appl. Phys. Lett. **92**, 022510 (2008).

[9]H. Tanigawa, T. Koyama, M. Bartkowiak, S. Kasai, K. Kobayashi, T. Ono, and Y. Nakatani, Phys. Rev. Lett. **101**, 207203 (2008).

[10]Y. Nakatani, A. Thiaville, and J. Miltat, J. Magn. Magn. Mater. **290–291**, 750 (2005).

[11]M. Klaui, C. A. F. Vaz, J. A. C. Bland, L. J. Heyderman, F. Nolting, A. Pavlovska, E. Bauer, S. Cherifi, S. Heun, and A. Locatelli, Appl. Phys. Lett. **85**, 5637 (2004).

[12]M. Hayashi, L. Thomas, C. Rettner, R. Moriya, X. Jiang, and S. S. P. Parkin, Phys. Rev. Lett. **97**, 207205 (2006).

[13]O. Tchernyshyov and G. W. Chern, Phys. Rev. Lett. **95**, 197204 (2005).

[14]J. He, Z. Li, and S. Zhang, Phys. Rev. B **73**, 184408 (2006).

[15]O. A. Tretiakov, D. Clarke, Gia-Wei Chern, Ya. B. Bazaliy, and O. Tchernyshyov, Phys. Rev. Lett. **100**, 127204 (2008).

[16]The micromagnetic calculation has been performed in a nanowire of 300 nm width and 20 nm thickness with material parameters of $Ni_{80}Fe_{20}$: saturation magnetization Ms = 800 emu/cm^3, exchange stiffness $A^* = 1.3 \times 10^{-6}$ erg/cm damping constant $\alpha = 0.01$. The unit cell dimension of the model is $4 \times 4 \times 20$ nm^3. The H_{WB} obtained from this model calculation was 7 Oe similar to the experimentally obtained value.

[17]A. A. Thiele, Phys. Rev. Lett. **30**, 230 (1973).

[18]M. Hayashi, L. Thomas, C. Rettner, R. Moriya, and S. S. P. Parkin, Nature Phys. **3**, 21 (2007).